Dynamic jamming of iceberg-choked fjords

Ivo R. Peters[1], Jason M. Amundson[2], Ryan Cassotto[3], Mark Fahnestock[4], Kristopher N. Darnell[5], Martin Truffer[4], and Wendy W. Zhang[1]

[1] James Franck Institute and Department of Physics, University of Chicago, Chicago, Illinois, USA, [2] Department of Natural Sciences, University of Alaska Southeast, Juneau, Alaska, USA, [3] Department of Earth Sciences, University of New Hampshire, Durham, New Hampshire, USA, [4] Geophysical Institute, University of Alaska Fairbanks, Fairbanks, Alaska, USA, [5] Jackson School of Geosciences and Institute for Geophysics, University of Texas at Austin, Austin, Texas, USA

Abstract We investigate the dynamics of ice mélange by analyzing rapid motion recorded by a time-lapse camera and terrestrial radar during several calving events that occurred at Jakobshavn Isbræ, Greenland. During calving events (1) the kinetic energy of the ice mélange is 2 orders of magnitude smaller than the total energy released during the events, (2) a jamming front propagates through the ice mélange at a rate that is an order of magnitude faster than the motion of individual icebergs, (3) the ice mélange undergoes initial compaction followed by slow relaxation and extension, and (4) motion of the ice mélange gradually decays before coming to an abrupt halt. These observations indicate that the ice mélange experiences widespread jamming during calving events and is always close to being in a jammed state during periods of terminus quiescence. We therefore suspect that local jamming influences longer timescale ice mélange dynamics and stress transmission.

1. Introduction

Recent studies [e.g., *Joughin et al.*, 2008; *Amundson et al.*, 2010; *Howat et al.*, 2010; *Walter et al.*, 2012; *Seale et al.*, 2011; *Sundal et al.*, 2013; *Foga et al.*, 2014] have suggested that ice mélange, or dense packs of icebergs and sea ice found in proglacial fjords, can influence calving of icebergs from tidewater glaciers on seasonal timescales. Variations in glacier length due to seasonal variations in calving can be on the order of several kilometers. Consequently, ice mélange may indirectly affect the stability of tidewater glaciers due to the nonlinear relationship between glacier geometry and glacier dynamics [*Joughin et al.*, 2012].

Ice mélange forms when ocean currents and surface winds are unable to efficiently evacuate icebergs from a fjord. The persistence of ice mélange is a function of iceberg productivity, fjord geometry, and sea ice formation. At some fjords, ice mélange exists only when air and water temperatures are low enough to permit the growth of a thick sea ice matrix [*Howat et al.*, 2010; *Walter et al.*, 2012]. At others, a combination of high iceberg productivity and confining fjord geometry enables ice mélange to persist year round as a result of iceberg-iceberg and iceberg-bedrock contact forces [see also *Geirsdóttir et al.*, 2008; *Jakobsson et al.*, 2012].

Several observations suggest that ice mélange can be viewed as a weak, granular ice shelf capable of exerting resistive stresses onto a glacier terminus [*Thomas*, 1979; *Johnson et al.*, 2004] and influencing iceberg calving. First, seasonal variations in calving rates are well correlated with the formation and dispersal of ice mélange (or changes in mobility) [*Sohn et al.*, 1998; *Reeh et al.*, 2001; *Joughin et al.*, 2008; *Howat et al.*, 2010; *Seale et al.*, 2011; *Walter et al.*, 2012; *Cassotto et al.*, 2015]. Second, during periods of terminus quiescence, ice mélange is pushed from behind by the advance of the glacier terminus (i.e., the ice mélange must also push back against the terminus) [*Joughin et al.*, 2008; *Amundson et al.*, 2010; *Sundal et al.*, 2013; *Foga et al.*, 2014]. Third, complete dispersal of ice mélange appears to cause a small increase in glacier velocity that is comparable to tidally induced velocity variations [*Walter et al.*, 2012]. Finally, observations and theoretical work suggest that resistive forces from ice mélange do not need to be large to hold together heavily fractured termini [*Reeh et al.*, 2001; *Amundson et al.*, 2010].

The slow and steady motion of ice mélange observed between calving events belies its dynamic and variable behavior. For example, large calving events at Jakobshavn Isbræ cause icebergs in the fjord to quickly accelerate to speeds of about 1 m/s (an increase in speed by 3 orders of magnitude). Following

calving events, the ice mélange moves slower than the glacier but gradually accelerates over the subsequent days until it reaches the same speed as the glacier terminus [*Amundson et al.*, 2010]. These observations suggest that ice mélange undergoes temporal variations in strain that are modulated by terminus activity.

The rheology of ice mélange is unknown, and therefore, it is not currently possible to calculate the resistance provided by ice mélange or fully evaluate its impact on tidewater glacier dynamics. To gain insights into its rheology, we collected high temporal and spatial resolution time-lapse photography and terrestrial radar data at Jakobshavn Isbræ during a 2 week period in summer 2012. We focus our analysis on rapid motion of ice mélange that was observed during several full-glacier thickness calving events.

We analyze our data in light of the recent discovery of dynamic jamming fronts, a phenomenon that occurs in granular systems that are close to the jamming point. A granular system with a packing fraction ϕ below the jamming point ϕ_J can flow but becomes rigid when the packing fraction reaches or exceeds the jamming point [*Cates et al.*, 1998; *Liu and Nagel*, 1998; *Reichhardt and Olson Reichhardt*, 2014]. An important difference between a jammed solid and a regular solid is that the stress is not spatially homogeneous but concentrated in force chains. This results in a distribution of stresses, with an increased probability of finding very high locally concentrated stresses [*Liu et al.*, 1995; *Majmudar and Behringer*, 2005]. The packing fraction (in two dimensions) is defined as the area occupied by the particles divided by the total system area, and the jamming point depends on the dimensions of the system and particle properties like shape and friction coefficient. The packing fraction has traditionally been treated as a global property in the context of jamming. However, recent experiments have shown that the transition to a jammed state can occur as a transient process in which a strong perturbation causes a closely packed system to jam locally and for the jammed region to quickly spread throughout the system [*Liu et al.*, 2010; *van Hecke*, 2012; *Waitukaitis and Jaeger*, 2012; *Waitukaitis et al.*, 2013; *Burton et al.*, 2013; *Peters and Jaeger*, 2014]. In this context it is more useful to treat the packing fraction as a local property. The details of dynamic jamming, and the types of systems in which it occurs, are only beginning to be explored. Here we will show that dynamic jamming occurs in closely packed ice mélange, a system that is orders of magnitude larger than other systems in which dynamic jamming has been observed.

2. Methods

We operated a high-rate time-lapse camera and a terrestrial radar interferometer at Jakobshavn Isbræ (Figure 1) from 30 July to 13 August 2012. The instruments recorded the motion of the ice mélange and glacier terminus area during several calving events.

The time-lapse camera system consisted of a Canon EOS 40D camera with a 28 mm lens, a Canon Timer Remote Controller (TC-80N3), and a custom-built power supply. The camera was oriented toward the glacier terminus and took one photo every 10 s. The camera clock was set to GPS time and was adjusted every couple of days to correct for clock drift.

A Gamma Remote Sensing GPRI-II radar interferometer [*Werner et al.*, 2008, 2012; *Dixon et al.*, 2012] was used to image the glacier and proglacial fjord. The GPRI-II is a Ku-band ($\lambda = 1.74$ cm) radial scanner with a range resolution of 0.75 m and an azimuth resolution of 0.4° (i.e., 7 m at a range of 1 km) and is capable of resolving millimeter-scale deformation via differences in electromagnetic phase. However, rapid motion of the ice mélange during calving events results in incoherence, which precludes measurement of the interferometric phase. Therefore, our analysis is based on the radar backscatter signal, also referred to as multilook intensity images. The radar performed 162° scans using a 16 km radius; it scanned every 3 min except for during a few hours of high winds. Radar backscatter data were reprojected to 15 m Cartesian space using slant range. Given the low-grazing angle of the radar in this application, the difference between slant range and horizontal range is less than 1%.

The time-lapse photography and radar data sets are complementary and together provide a comprehensive view of the ice mélange motion during calving events. We analyzed both data sets using a particle image velocimetry (PIV) algorithm to obtain velocity fields. Due to a poor look angle and poor ground control, pixel displacements in the time-lapse photos were not translated into true ground displacements. When processing the time-lapse photos we used a correlation window size of 40×40 pixels. We analyzed the radar data by first using a coarse PIV pass (correlation window size of 64×64 pixels) to be able to detect large
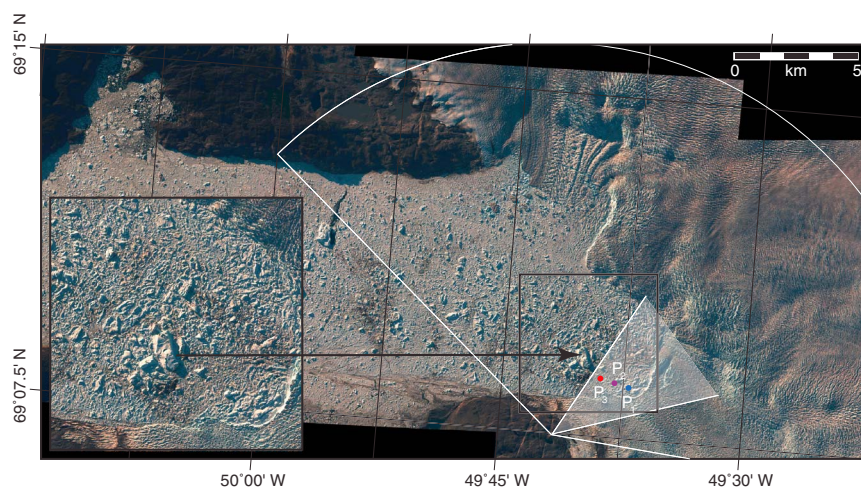
Figure 1. WorldView-2 image of Ilulissat Icefjord and the terminus of Jakobshavn Isbræ, acquired on 6 July 2010 (copyright 2010 Digital Globe, Inc.). The areas covered by the terrestrial radar and the time-lapse camera are indicated by the semicircular wedge and the shaded triangle, respectively. The inset shows a close-up of the near-terminus region. The blue, purple, and red dots (P_1–P_3) indicate the approximate geographic coordinates of the pixels that were tracked in the time-lapse photographs and presented in Figure 3c.

displacements, which we subsequently refined in two steps down to 32×32 pixels for increased spatial resolution.

3. Observations of Ice Mélange Motion

We observed seven full-glacier thickness calving events (e.g., Movie S1 in the supporting information). During these events, one to several icebergs with spatial dimensions of hundreds of meters detach from the glacier and subsequently capsize. The detachment and capsize of each iceberg lasts about 5 min; rapid motion of ice mélange generally continues for 30–60 min and often terminates abruptly [see also *Amundson et al.*, 2008; *James et al.*, 2014].

3.1. Jamming Front and Kinetic Energy

The velocity fields derived from time-lapse photography and terrestrial radar data allow us to determine how quickly motion induced by the calving event spreads through the ice mélange (Movie S2). Figure 2 shows snapshots of the calculated velocity field during a typical calving event. The calving event induced motion in the innermost fjord concurrent with the detachment and capsize of the calving iceberg. The area of the ice mélange that was affected rapidly expanded far down fjord during the following minutes.

To quantify the spreading of the motion in the ice mélange, we determine the velocity profile along a line from the terminus to the end of the field of view of the radar. Figure 3a shows the velocity profile along this transect at five instances in time, with 3 min between each curve. During the first 9 min, a clear front can be ob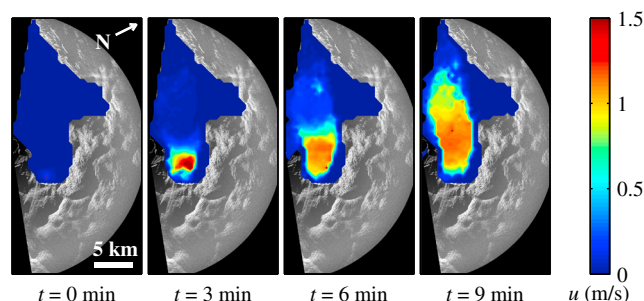served propagating down fjord; some acceleration of the ice mélange occurs prior to the arrival of this front, as can be seen in the purple ($t = 6$ min) curve between about 7 to 12 km down fjord. Later, the motion dissipates, resulting in an overall decrease in velocity and the front becoming more difficult to identify. The sudden increase in velocity when the front passes and the subsequent slow relaxation can be seen more clearly by measuring the velocities at specific distances from the terminus and plotting the velocity as a function

Figure 2. Time evolution of the ice mélange velocity field, derived from PIV analysis of radar backscatter data, from a full-glacier thickness calving event that occurred on 2 August 2012; $t = 0$ min corresponds to 23:08:30 UTC. See also Movie S2.
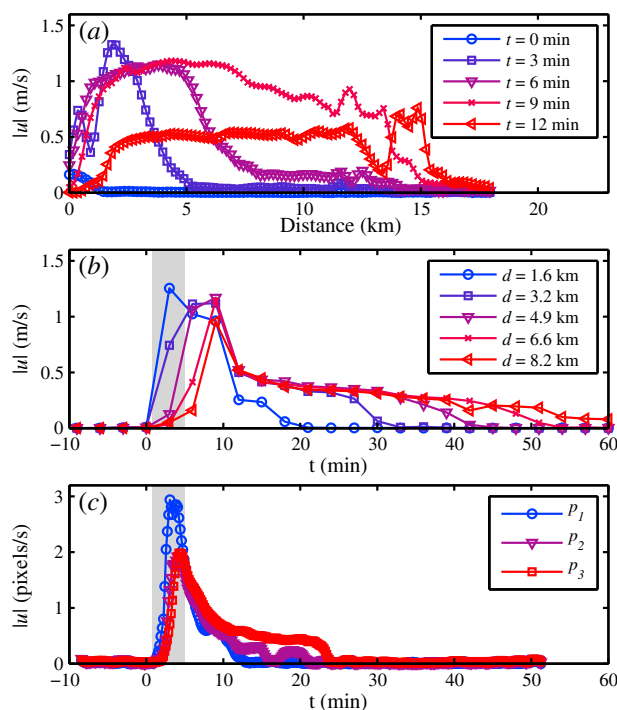
Figure 3. Ice mélange velocities from the calving event presented in Figure 2. (a) Velocity profiles along the ice mélange during and after the calving event. The glacier terminus is at $x = 0$. (b) Velocity as a function of time at various distances from the terminus. (c) Pixel velocities (from time-lapse photography) at increasing distances from the terminus (from P_1 to P_3). See also Figure 1 and Movie S1. In Figures 3b and 3c, the gray box indicates the period of time during which icebergs are actively calving from the terminus.

of time (Figures 3b and 3c). The sudden increase in velocity occurs at a later time at points farther from the glacier. Whereas the acceleration occurs throughout the ice mélange within 10 min, the relaxation is spread out over about 40 min and is slower down fjord. Using a speed threshold of 0.5 m/s, we determine the position of the front in each frame, from which we determine a typical speed at which the front propagates. We calculated front propagation speeds in the range of 16 to 20 m/s, an order of magnitude faster than the typical speeds of individual icebergs. Variations in front speeds may reflect variations in packing fraction or forcing mechanism (see section 4).

We also estimate the amount of kinetic energy, K, as a function of time in the ice mélange by evaluating $K = \frac{1}{2}\rho_i h \int \int (u_x^2 + u_y^2)\mathrm{d}x\mathrm{d}y$, where $\rho_i = 917$ kg/m^3 is the density of ice, $h \sim 100$ m is the thickness of the ice mélange (iceberg freeboard ranges from about 1 m to greater than 10 m), and $\mathbf{u} = \langle u_x, u_y \rangle$ is the velocity field. We neglect the motion of water in our calculations. Peak kinetic energies are on the order of 10^{12} J, which is 2 orders of magnitude smaller than the amount of energy that is released by the calving events [*MacAyeal et al.*, 2011; *Burton et al.*, 2012].

3.2. Strain

We employed a Voronoi analysis [*Aurenhammer et al.*, 2013] to investigate whether the ice mélange experiences extension or compression during the calving event because we found that the velocity fields (Figure 2) were too noisy to be used for calculating spatial derivatives. To generate Voronoi diagrams, we developed a tracking algorithm, based on cross correlations, that allowed us to select several large and easily identifiable icebergs (reference points) in one radar image and track it through the subsequent images. To improve performance, the algorithm used the PIV data (Figure 2) as an initial guess for the displacement to limit the searching area. The Voronoi cells were then computed by determining the proximity of the selected icebergs to each pixel in the image (see inset in Figure 4).

During the propagation of the jamming front there is an overall compaction that occurs in about 10 min. The fast compaction is followed by a slow relaxation process with a typical timescale of 1 h. The packing fraction of the tracked region typically decreases after the relaxation phase. The initial compaction represents the total compaction of the entire tracked region, including a portion of the ice mélange to the north that does not experience any motion during the calving event (see Movie S2), and therefore underestimates local compaction that occurs as the jamming front passes through the ice mélange. Noise in the data prevents us from calculating local compaction. We therefore only use the fractional changes in the areas of the Voronoi cells for order-of-magnitude comparisons with theoretical work on jamming. The total compaction and relaxation and the timescales of ice mélange motion differed between calving events, but all events exhibited the same qualitative behavior.
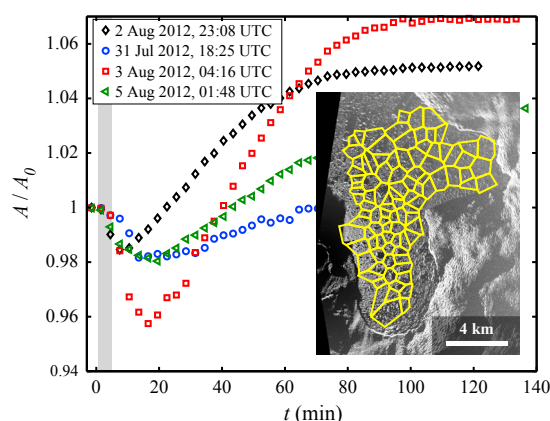
Figure 4. Voronoi cell analysis reveals that the total surface area of the ice mélange decreases immediately following calving events (at $t \approx 0$) and then slowly expands. Compaction and relaxation are shown for four calving events. The black diamonds and gray box correspond to the calving event presented in Figures 2 and 3; the inset shows the distribution of the Voronoi cells for that event at $t = 0$.

4. Interpretation

We have observed large calving events causing the rapid growth and down fjord propagation of a compacted region of ice mélange that moves at a nearly uniform speed. Similar behavior has been observed in other types of dense particulate systems subjected to compressive forcings, such as two-dimensional packing of frictional disks [*Waitukaitis et al.*, 2013] and temporary solidification of a layer of dense corn starch suspension floating on oil [*Peters and Jaeger*, 2014]. Despite great differences in characteristic scales and composition, these systems are composed of fairly rigid constituents that strongly resist compression through force chains when jammed together but offer negligible resistance when there is finite interstitial spacing between them. Strong compressive stresses cause an initial reduction in the interstitial spacings, but eventually, the constituents jam together and prevent further compression. The particulate systems respond by propagating the jammed region over an increasingly larger area.

The similarity between these systems suggests the following interpretation of the observed ice mélange motion. Between calving events the ice mélange is closely packed but is not at the jamming point everywhere (i.e., the fjord is not uniformly jammed). Jamming may still occur locally and have important consequences for stress transmission and ice mélange motion. When an iceberg calves, it pushes the icebergs in the inner fjord and compresses the ice mélange locally, causing the local packing fraction to rapidly increase until it reaches the jamming point. As a result, there is a large area of ice mélange that moves as a single solid mass, which then compresses the ice mélange farther down fjord and causes the area of rapid motion to expand. This process continues as long as there is a driving force from the calving iceberg or enough inertia in the jammed region and can be observed as a jamming front traveling down the fjord at a speed much larger than the speed of the calving iceberg. The jamming front is defined as the region that delineates the jammed regions from the unjammed region down fjord. Friction between icebergs and hydrodynamic drag eventually cause the ice mélange to gradually decelerate, but only after some relaxation and expansion has occurred.

The dynamic jamming scenario allows for a quantitative prediction for how quickly the jammed region should grow in response to a compressive forcing. Under compression, the spacing between icebergs reduces because water can freely flow out of the interstitial spacings and because icebergs may be able to partially raft over each other, undergo rotations, and/or fracture. After an initial compaction the mechanical resistance greatly increases and the icebergs become jammed. A reasonable first approximation of the ice mélange motion is that only the area occupied by the water contracts under compression and that the map view area occupied by icebergs is conserved. Corrections to this approximation could be made by taking into account the aforementioned processes involving the motion of the icebergs (e.g., by including terms for rotations or mechanical failure of icebergs). Thus, if ϕ is the two-dimensional solid packing fraction, then conservation of iceberg area requires

$$\frac{\partial \phi}{\partial t} + \nabla \cdot (\phi \mathbf{u}) = 0. \tag{1}$$

Below the jamming point, ϕ_J, the ice mélange contracts while offering only a small amount of resistance (from friction and hydrodynamic drag). Once ϕ reaches ϕ_J, the resistance to any further significant compression jumps discontinuously and becomes far larger than the typical forcing. Continued forcing creates a jammed region at ϕ_J that grows in spatial extent.

To estimate the speed of the jamming front, u_f, we make the following simplifying assumptions: (i) the velocity field within the jammed region of the ice mélange is a spatially uniform one-dimensional translation

with icebergs moving at speed u_J, (ii) the entire jammed region is at ϕ_J, and (iii) down fjord from the jammed region, the ice mélange is barely disturbed and therefore reasonably approximated as a region of zero flow at a uniform initial packing fraction ϕ_0. The measured velocity profiles within the ice mélange (Figure 3a) are consistent with these simplifications.

Conservation of iceberg area then simplifies to a jump condition across the moving front of the jammed region. This condition is most simply enforced by switching to a comoving reference frame in which the jamming front appears stationary: icebergs ahead of the jamming front have speed $-u_f$, icebergs behind the jamming front have speed $-u_f + u_J$, and $\partial\phi/\partial t = 0$. Thus, integrating equation (1) across the jamming front yields the jump condition

$$-\phi_0 u_f - \phi_J(-u_f + u_J) = 0, \tag{2}$$

which rearranges to give

$$u_f = u_J\left(\frac{\phi_J}{\phi_J - \phi_0}\right). \tag{3}$$

Due to the chaotic nature of ice mélange, we cannot readily calculate packing fractions from our images. In two dimensions, the packing fraction is defined as

$$\phi = \frac{A_{\text{ice}}}{A}, \tag{4}$$

where A_{ice} is the effective area occupied by ice within a control area A. The control area can change dynamically due to compression, but the area occupied by icebergs remains constant under our first-order approximation (equation (1)). Plugging equation (4) into equation (3) and rearranging gives

$$u_f = u_J\left(\frac{1}{1 - \frac{A_J}{A_0}}\right), \tag{5}$$

where A_0 is the initial control area and A_J is the control area after becoming jammed. Equation (5) indicates that the speed of the jamming front is determined by the proximity of the initial packing fraction to the jamming point. From our observed front speeds of 16–20 m/s and typical horizontal speeds of individual icebergs of the order of 1 m/s (Figure 2) [see also *Amundson et al.*, 2010], we estimate the numerical value of A_J/A_0 to be 0.94–0.95. This corresponds to compression of 5–6%, which is in agreement with the order of magnitude compression shown in Figure 4 and therefore gives further evidence that dynamic jamming occurs in ice mélange during large-scale calving events.

5. Conclusions

Analysis of time-lapse photography and terrestrial scanning radar data from Jakobshavn Isbræ indicates that large portions of proglacial ice mélange compact and become uniformly jammed during calving events. A jamming front, which delineates jammed and unjammed portions of the fjord, propagates down fjord at about 20 m/s, or roughly an order of magnitude faster than individual icebergs. After calving activity ceases the ice mélange slowly relaxes and decelerates before coming to an abrupt halt. The initial compaction and rapid jamming front are consistent with laboratory studies of jamming in a variety of systems, which together indicate that the ice mélange must be close to the jamming point prior to the initiation of the calving events.

The proximity of the ice mélange to the jamming point suggests that transient jamming events may occur during periods of terminus quiescence, causing the ice mélange resistance to frequently transition from a spatially smooth, fluid-like distribution of an unjammed state to a spatially highly heterogeneous distribution. Studies from condensed matter physics show that, upon jamming, most of the loading experienced by a quasi two-dimensional system is transmitted across the system along force chains. In ice mélange, the force chains are composed of icebergs in physical contact that transmit resistance from the fjord walls to the glacier terminus. This concentrated form of force transmission causes the terminus facing a jammed region of ice mélange to experience large resistive stresses at a few highly localized spots where force chains end while leaving the rest unaffected. As a result the peak resistance obtained at the ends of force chains is

significantly larger than what a single smooth block of ice with comparable dimensions can exert. Assessing the cumulative effect of these small-scale jamming events requires comparison of long-timescale (hours to days) observations of ice mélange motion with laboratory experiments and discrete particle models.

Two features of our data, the moderate acceleration of icebergs that precedes arrival of the jamming front and the abrupt halt in motion at the end of the events, have not been observed in other systems and cannot be explained by a simple theory of dynamic jamming. A complete theory of dynamic jamming in ice mélange needs to be able to describe these observations and account for the possibility that the jamming point varies seasonally, that the packing fraction is influenced by mechanical failure and/or melting of icebergs, and that hydrodynamic forces affect jamming processes.

Ice mélange is easily the largest system that has been observed to experience dynamic jamming. In fact, it is difficult to imagine other granular systems on Earth that contain larger constituents. Our study of jamming on the meter-to-kilometer scale is complementary to current efforts in condensed matter physics to extend jamming from macroscopic particulate systems down to the micron-scale and molecular systems (e.g., colloids and block-copolymer lipid system in langmuir troughs). We expect the extrapolation to larger length scales will reveal new regimes of jamming dynamics not accessible in systems with smaller constituents. Furthermore, given the potential impact of ice mélange on iceberg calving and glacier stability, this work motivates further investigation of jamming and stress transmission through ice mélange and other quasi two-dimensional materials.

References

Amundson, J. M., M. Truffer, M. P. Lüthi, M. Fahnestock, M. West, and R. J. Motyka (2008), Glacier, fjord, and seismic response to recent large calving events, Jakobshavn Isbræ, Greenland, *Geophys. Res. Lett.*, *35*, L22501, doi:10.1029/2008GL035281.

Amundson, J. M., M. Fahnestock, M. Truffer, J. Brown, M. P. Lüthi, and R. J. Motyka (2010), Ice mélange dynamics and implications for terminus stability, Jakobshavn Isbræ, Greenland, *J. Geophys. Res.*, *115*, F01005, doi:10.1029/2009JF001405.

Aurenhammer, F., R. Klein, and D.-T. Lee (2013), *Voronoi Diagrams and Delaunay Triangulations*, 348 pp., World Sci., N. J.

Burton, J. C., J. M. Amundson, D. S. Abbot, A. Boghosian, L. Mac Cathles, S. Correa-Legisos, K. N. Darnell, N. Guttenberg, D. M. Holland, and D. R. MacAyeal (2012), Laboratory investigations of iceberg-capsize dynamics, energy dissipation, and tsunamigenesis, *J. Geophys. Res.*, *117*, F01007, doi:10.1029/2011JF002055.

Burton, J. C., P. Y. Lu, and S. R. Nagel (2013), Energy loss at propagating jamming fronts in granular gas clusters, *Phys. Rev. Lett.*, *111*, 188001, doi:10.1103/PhysRevLett.111.188001.

Cassotto, R., M. Fahnestock, J. M. Amundson, M. Truffer, and I. Joughin (2015), Seasonal and interannual variations in ice mélange rigidity and its impact on terminus stability, Jakobshavn Isbræ, Greenland, *J. Glaciol.*, *61*(225), 76–88, doi:10.3189/2015JoG13J235.

Cates, M., J. Wittmer, J.-P. Bouchaud, and P. Claudin (1998), Jamming, force chains, and fragile matter, *Phys. Rev. Lett.*, *81*, 1841–1844, doi:10.1103/PhysRevLett.81.1841.

Dixon, T. H., D. Voytenko, C. Lembke, S. de laPeña, I. Howat, N. Gourmelen, C. Werner, and B. Oddsson (2012), Emerging technology monitors ice-sea interface at outlet glaciers, *Eos Trans. AGU*, *93*(48), 497–498.

Foga, S., L. A. Stearns, and C. J. van der Veen (2014), Techniques to quantify terminus and ice mélange behavior at Helheim Glacier, East Greenland, *Mar. Technol. Soc. J.*, *48*(5), 81–91.

Geirsdóttir, A., G. H. Miller, N. J. Wattrus, H. Björnsson, and K. Thors (2008), Stabilization of glaciers terminating in closed water bodies: Evidence and broader implications, *Geophys. Res. Lett.*, *35*, L17502, doi:10.1029/2008GL034432.

Howat, I. M., J. E. Box, Y. Ahn, A. Herrington, and E. M. McFadden (2010), Seasonal variability in the dynamics of marine-terminating outlet glaciers in Greenland, *J. Glaciol.*, *56*(198), 601–613.

Jakobsson, M., J. B. Anderson, F. O. Nitsche, R. Gyllencreutz, A. E. Kirshner, N. Kirchner, M. O'Regan, R. Mohammed, and B. Eriksson (2012), Ice sheet retreat dynamics inferred from glacial morphology of the central Pine Island Bay Trough, West Antarctica, *Quat. Sci. Rev.*, *38*, 1–10, doi:10.1016/j.quascirev.2011.12.017.

James, T. D., T. Murray, N. Selmes, K. Scharrer, and M. O'Leary (2014), Buoyant flexure and basal crevassing in dynamic mass loss at Helheim Glacier, *Nat. Geosci.*, *7*, 593–596, doi:10.1038/ngeo2204.

Johnson, J. V., P. R. Prescott, and T. J. Hughes (2004), Ice dynamics preceding catastrophic disintegration of the floating part of Jakobshavn Isbræ, Greenland, *J. Glaciol.*, *50*(171), 492–504.

Joughin, I., I. M. Howat, M. Fahnestock, B. Smith, W. Krabill, R. B. Alley, H. Stern, and M. Truffer (2008), Continued evolution of Jakobshavn Isbræ following its rapid speedup, *J. Geophys. Res.*, *113*, F04006, doi:10.1029/2008JF001023.

Joughin, I., B. E. Smith, I. M. Howat, D. Floricioiu, R. B. Alley, M. Truffer, and M. Fahnestock (2012), Seasonal to decadal scale variations in the surface velocity of Jakobshavn Isbræ, Greenland: Observations and model-based analysis, *J. Geophys. Res.*, *117*, F02030, doi:10.1029/2011JF002110.

Liu, A. J., and S. R. Nagel (1998), Jamming is not just cool any more, *Nature*, *396*, 21–22.

Liu, B., M. Shelley, and J. Zhang (2010), Focused force transmission through an aqueous suspension of granules, *Phys. Rev. Lett.*, *105*, 188301, doi:10.1103/PhysRevLett.105.188301.

Liu, C.-H., S. R. Nagel, D. A. Schecter, S. N. Coppersmith, S. Majumdar, O. Narayan, and T. A. Witten (1995), Force fluctuations in bead packs, *Science*, *269*, 513–515.

MacAyeal, D. R., D. S. Abbot, and O. V. Sergienko (2011), Iceberg-capsize tsunamigenesis, *Ann. Glaciol.*, *52*(58), 51–56.

Majmudar, T. S., and R. P. Behringer (2005), Contact force measurements and stress-induced anisotropy in granular materials, *Nature*, *435*, 1079–1082, doi:10.1038/nature03805.

Peters, I. R., and H. M. Jaeger (2014), Quasi-2D dynamic jamming in cornstarch suspensions: Visualization and force measurements, *Soft Matter*, *10*, 6564–6570, doi:10.1039/c4sm00864b.

Reeh, N., H. H. Thomsen, A. K. Higgins, and A. Weidick (2001), Sea ice and the stability of north and northeast Greenland floating glaciers, *Ann. Glaciol.*, *33*, 474–480.

Reichhardt, C., and C. J. Olson Reichhardt (2014), Aspects of jamming in two-dimensional athermal frictionless systems, *Soft Matter*, *10*, 2932–2944, doi:10.1039/C3SM53154F.

Seale, A., P. Christofferson, R. I. Mugford, and M. O'Leary (2011), Ocean forcing of the Greenland Ice Sheet: Calving fronts and patterns of retreat identified by automatic satellite monitoring of eastern outlet glaciers, *J. Geophys. Res.*, *116*, F03013, doi:10.1029/2010JF001847.

Sohn, H.-G., K. C. Jezek, and C. J. van der Veen (1998), Jakobshavn Glacier, west Greenland: 30 years of spaceborne observations, *Geophys. Res. Lett.*, *25*(14), 2699–2702.

Sundal, A. V., A. Shepherd, M. Van den Broeke, J. Van Angelen, N. Gourmelen, and J. Park (2013), Controls on short-term variations in Greenland glacier dynamics, *J. Glaciol.*, *59*(217), 883–892, doi:10.3189/2013JoG13J019.

Thomas, R. H. (1979), Ice shelves: A review, *J. Glaciol.*, *24*(90), 273–286.

van Hecke, M. (2012), Running on cornflour, *Nature*, *487*, 174–175, doi:10.1038/487174a.

Waitukaitis, S. R., and H. M. Jaeger (2012), Impact-activated solidification of dense suspensions via dynamic jamming fronts, *Nature*, *487*, 205–209, doi:10.1038/nature11187.

Waitukaitis, S. R., L. K. Roth, V. Vitelli, and H. M. Jaeger (2013), Dynamic jamming fronts, *Europhys. Lett.*, *102*, 44001, doi:10.1209/0295-5075/102/44001.

Walter, J. I., J. E. Box, S. Tulaczyk, E. E. Brodsky, I. M. Howat, Y. Ahn, and A. Brown (2012), Oceanic mechanical forcing of a marine-terminating Greenland glacier, *Ann. Glaciol.*, *53*(60), 181–192, doi:10.3189/2012AoG60A083.

Werner, C., T. Strozzi, A. Wiesmann, and U. Wegmüller (2008), Gamma's portable radar interferometer, paper presented at 13th FIG Symposium on Deformation and Analysis, 4th IAG Symposium on Geodesy for Geotechnical and Structural Engineering, pp. 1–10, Lisbon, 12–15 May.

Werner, C., A. Wiesmann, T. Strozzi, A. Kos, R. Caduff, and U. Wegmüller (2012), The GPRI multi-mode differential interferometric radar for ground-based observations, in *Proceedings of the EUSAR 2012 – 9th European Conference on Synthetic Aperture Radar*, pp. 304–307, VDE, Nuremberg, Germany, 24–24 April.